Electronic Supplementary Material (ESI) for Nanoscale.

Supporting Information for

A stable superatomic $Cu_6(SMPP)_6$ nanocluster with dual emissions

Haiming Wu,[a] Rajini Anumula,[a] Gaya N. Andrew,[a] Zhixun Luo*[,a,b]

[a]Beijing National Laboratory for Molecular Sciences (BNLMS), State Key Laboratory for Structural Chemistry of Unstable and Stable Species, Institute of Chemistry, Chinese Academy of Sciences, Beijing 100190, China

[b]University of Chinese Academy of Sciences, Beijing 100049, China

*Corresponding Email: zxluo@iccas.ac.cn

This PDF file includes (Figs. S1-8; Tables S1-S6)**:**

S1. Experimental and theoretical methods

Chemicals and reagents. All chemicals are commercially available and used as received (without further purification), including cupric (II) acetate [$Cu(OAC)_2$, 99 %, Alfar Aesar], triphenylphosphine gold (I) chloride ($AuClPPh_3$, 98 %, Acros Organic), 2-mercapto-5-n-propylpyrimidine ($SN_2C_7H_{10}$, SMPP, 98 %, Alfar Aesar), sodium borohydride ($NaBH_4$, 98 %, Acros Organics), triethylamine (98 %, Acros Organics). The solvents mainly include dichloromethane (DCM for short below), methanol, n-hexane were purchased from Beijing Chemical Reagent Co. Ltd. The water used for the experiment was Milli-Q water, produced by a Millipore apparatus.

Synthesis of Cu_6 nanocluster. In a glass vial, $Cu(OAc)_2$ (15 mg) was dissolved completely in methanol (3 mL) under sonication. To this solution, 45 mg of SMPP was added in 3 mL DCM. Then a spot of $AuClPPh_3$ which dissolved in 2 mL DCM was added, by referring to a so-called "ion-induction" method.[1] The solution was cooled under an ice-bath. After stirring (~ 15 mins), 1 mL of cold $NaBH_4$ (45 mg/mL) and 25 μL of triethylamine were added together quickly to the above solution. This solution was kept under stirring and aged for one day at 0 ^oC and then was washed several times with distilled water. Afterwards, the solution was centrifuged by rotavapor and the obtained red extract was thus crystalized in DCM/hexane (1:4) at 4 ^oC and kept for dark orange single crystal growth for 15 days. The yield of Cu_6 was up to ~20 %.

Characterization. The single-crystal X-ray diffraction (XRD) data of the synthesized bimetallic Cu_6 nanocluster was measured on an Rigaku MM007HF Saturm724+ single crystal X-ray diffractometer with Mo Kα radiation (λ=0.71073 Å). Single crystal structure was solved by direct methods and refined with full-matrix-least-squares on F^2. High resolution of electrospray ionization time-of-flight mass spectrometry (ESI-TOF-MS) measurements was conducted by a Bruker Solarix 9.4T in the positive ionization mode. The UV-Vis absorption spectra were collected using an UV-3600 Shimadzu UV-Vis-NIR spectrophotometer. Photoluminescence spectra were recorded by a Horiba Scientific Fluoromax-4 spectrofluorometer. Luminescenec decay lifetimes and temperature-dependent spectra were recorded on an Edinburgh FLS980 spectrometer. X-ray photoelectron spectroscopy (XPS) was collected by a Thermo Fisher Scientific EscaLab250Xi spectrometer. Thermogravimetric analysis was recorded on a PerkinElmer Pyris1TGA.

Computational Methods. All the calculations were carried out with density functional theory (DFT) embedded in the Gaussian 09 software package.[2] Ground- and excited-state geometric structures of the Cu_6 NCs are optimized using B3LYP functional. The SDD pseudopotentials and basis sets are used for Cu atoms while all-electron def2-SVP basis sets are used for S, N, C, and H atoms. Vertical excitation and emission energies at optimized S_0 and S_1 structures were calculated using the TD-B3LYP method. Solvent effects (dichloromethane) were implicitly considered using the polarizable continuum model (PCM) for the TDDFT calculations. Natural population analysis (NPA) charges were analysized by Multiwfn software.[3] The canonical molecular orbitals were plotted with the VMD software.[4] Based on the

optimized structures by Gaussian09, total-energy calculations considering the scalar-relativistic effect were then carried out by using Amsterdam Density Functional (ADF) 2021.104 software, taking into account the zero-order regular approximation (ZORA). The interaction and chemical bonding nature were characterized by the energy decomposition analysis and natural orbitals for the chemical valence (EDA-NOCV) method based on B3LYP/TZ2P level of theory.[5]

S2. Experimental details

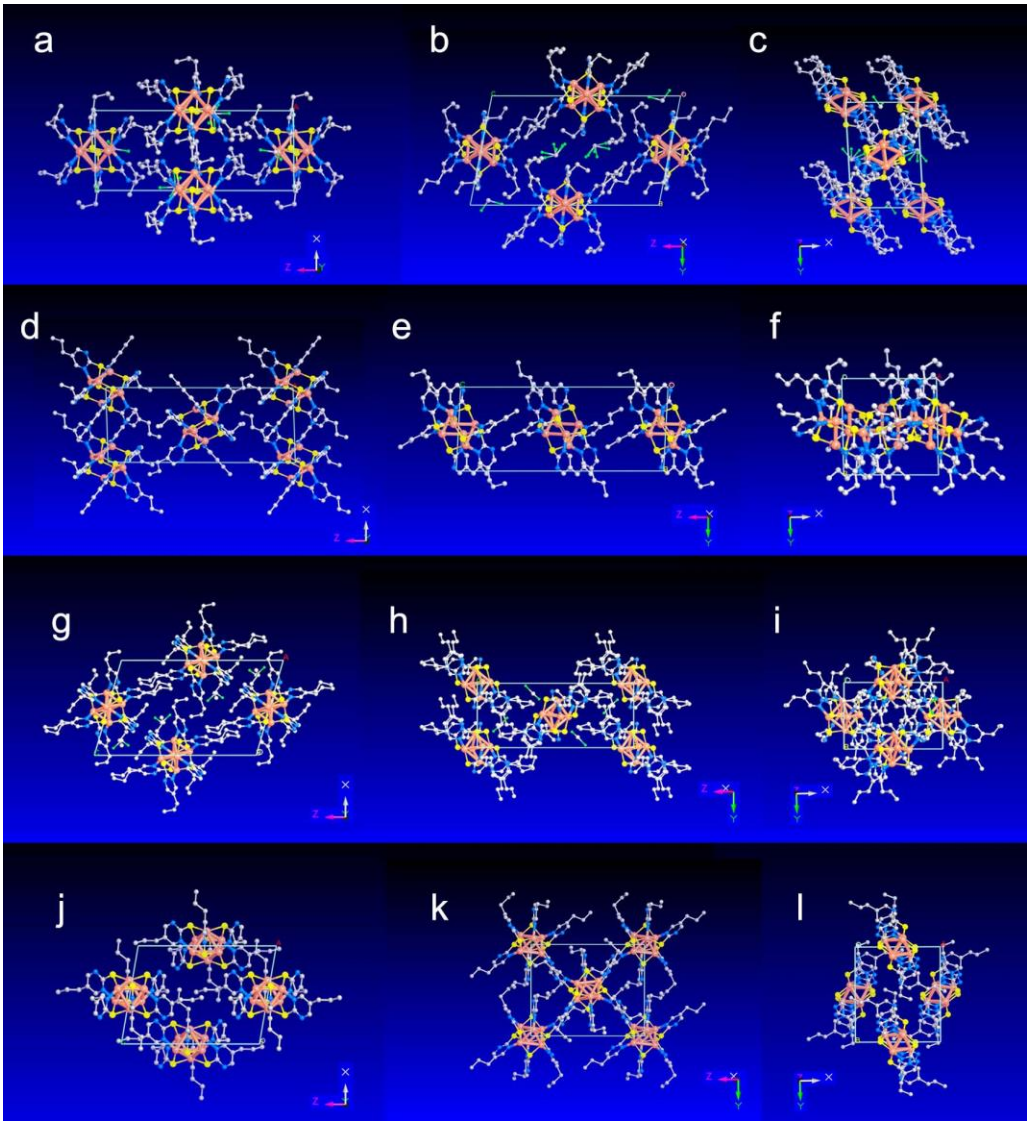

Fig. S1 Unit cell parsing of (a-c) **1**-**3** in this work and (d) **4** in ref.[6] Cu in orange, S yellow, N sky blue, C gray, Cl green. For clarity, H are omitted.

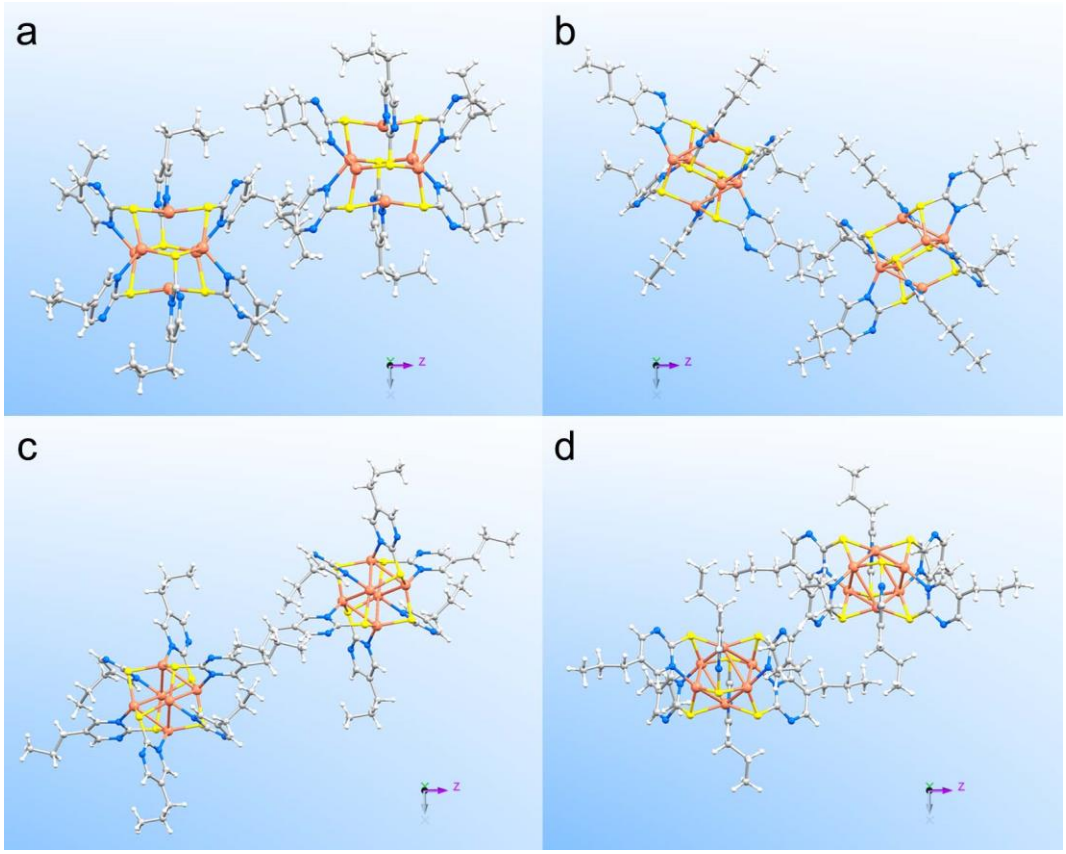

Fig. S2 Single-crystal structures of (a-c) **1**-**3** in this work and (d) **4** in ref.[6] Cu in orange, S yellow, N sky blue, C gray. For clarity, H white.

Table S1 Crystallographic data for $[Cu_6(SMPP)_6]$ nanocluster.

	1 in this work	**2** in this work	**3** in this work	**4** in Ref[6]
Empirical formula	$C_{44}H_{58.02}Cl_{4.03}Cu_6N_{12}S_6$	$C_{42}H_{54}Cu_6N_{12}S_6$	$C_{43.25}H_{56.51}Cl_{2.5}Cu_6N_{12}S_6$	$C_{42}H_{54}Cu_6N_{12}S_6$
Formula weight	1471.33	1300.57	1406.91	1300.56
Temperature (K)	293(2)	110.00(10)	110.00(10)	\
Crystal system	triclinic	triclinic	monoclinic	monoclinic
Space group	P-1	P-1	$P2_1/n$	$P2_1/n$
a (Å)	9.2167(4)	9.9012(4)	14.0232(11)	11.821(6)
b (Å)	13.7793(6)	10.0750(4)	9.1083(4)	13.032(6)
c (Å)	23.2892(7)	24.7923(7)	22.9694(16)	16.384(8)
α (deg)	78.740(3)	86.895(2)	90	90
β (deg)	88.981(3)	88.097(2)	105.853(7)	99.725(15)
γ (deg)	86.659(3)	88.605(3)	90	90
Volume ($Å^3$)	2895.81(19)	2467.52(16)	2822.2(3)	2488(2)
Z	2	2	2	4
ρ_{calc} (g/cm^3)	1.687	1.750	1.656	1.736
μ (mm^{-1})	2.609	2.839	2.603	2.816
F(000)	1489.0	1320.0	1425.0	1320
Crystal size (mm^3)	0.22 x 0.16 x 0.15	0.23 x 0.21 x 0.04	0.15 x 0.15 x 0.12	0.15 x 0.10 x 0.05
2Θ range for data collection (deg)	6.852 to 61.668	4.05 to 63.216	3.078 to 62.184	\
Index ranges	$-11 \le h \le 13$, $-19 \le k \le 19$, $-33 \le l \le 33$	$-14 \le h \le 14$, $-14 \le k \le 14$, $-35 \le l \le 35$	$-20 \le h \le 12$, $-10 \le k \le 12$, $-29 \le l \le 32$	\
Reflections collected	50454	13711	23116	20602
Independent reflections	16012 [R_{int} = 0.0459, R_{sigma} = 0.0576]	13711 [R_{int} = ?, R_{sigma} = 0.0634]	7609 [R_{int} = 0.0693, R_{sigma} = 0.0948]	\
Data / restraints / parameters	16012/327/733	13711/0/602	7609/401/421	\
Goodness-of-fit on F^2	1.150	1.128	1.103	0.929
Final R indexes [I>=2σ (I)]	R_1 = 0.1189, wR_2 = 0.3059	R_1 = 0.0724, wR_2 = 0.3059	R_1 = 0.1053, wR_2 = 0.2598	R_1 = 0.0546, wR_2 = 0.0781
Final R indexes [all data]	R_1 = 0.1457, wR_2 = 0.3213	R_1 = 0.0899, wR_2 = 0.1997	R_1 = 0.1579, wR_2 = 0.2899	\
Largest diff. peak/hole (e $Å^{-3}$)	3.78/-1.46	2.10/-1.20	3.31/-0.89	0.858/-0.661

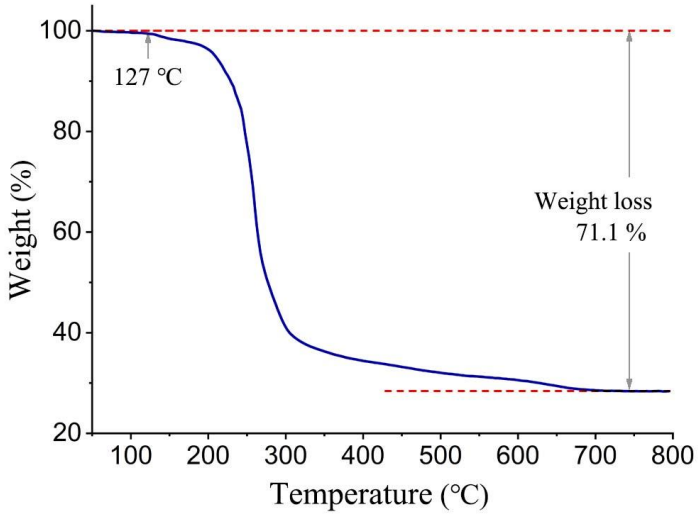

Fig. S3 TGA curve of $Cu_6(SMPP)_6$ NCs.

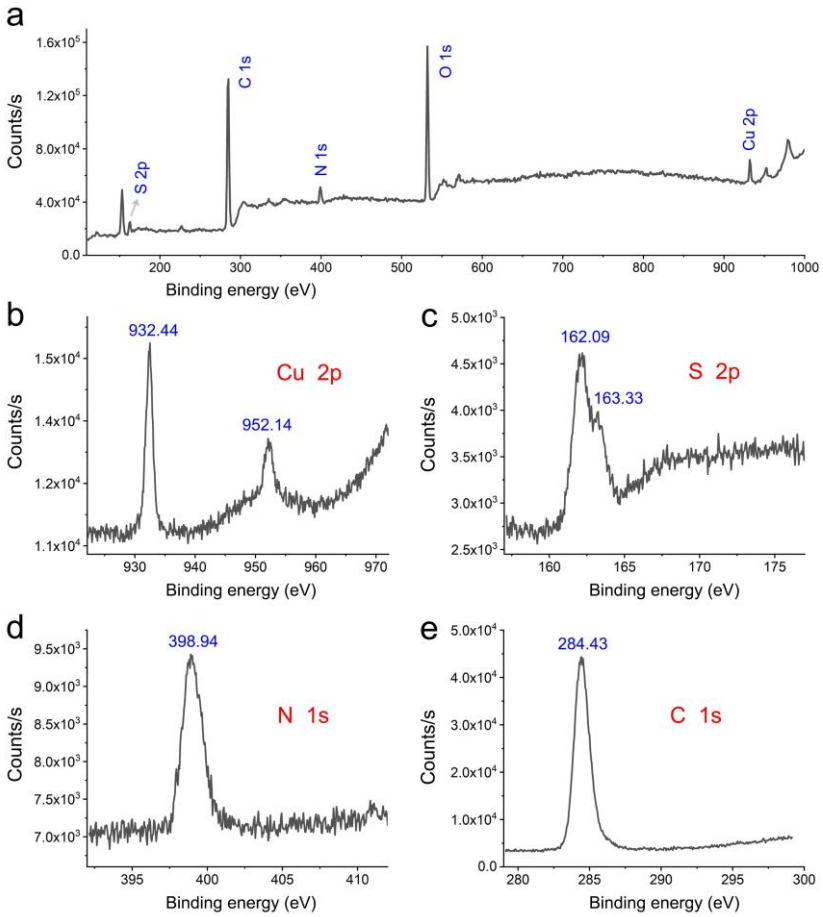

Fig. S4 (a) XPS survey spectrum of $Cu_6(SMPP)_6$ NCs. (b-e) High-resolution XPS spectra of Cu 2p, S 2p, N 1s and C 1s in the nanoclusters.

S3. Calculation details

3.1 Bond lengths

Table S2 Cu-Cu bond and Cu-S lengths (Å) in single-crystals 1-3 and DFT-optimized at the S_0 minima.

Bond	In **1**	In **2**	In **3**	DFT-optimized
Cu1-Cu2	2.93	3.16	2.92	2.66
Cu1-Cu3	2.97	2.73	2.89	2.64
Cu1-Cu5	2.90	3.18	2.88	2.64
Cu1-Cu6	2.91	3.45	2.94	2.66
Cu2-Cu3	2.69	2.81	2.73	2.64
Cu2-Cu4	2.90	3.18	2.88	2.64
Cu2-Cu6	3.24	3.46	3.20	2.66
Cu3-Cu4	2.91	3.45	2.94	2.66
Cu3-Cu5	3.24	3.46	3.20	2.66
Cu4-Cu5	2.93	3.16	2.92	2.66
Cu4-Cu6	2.97	2.73	2.89	2.64
Cu5-Cu6	2.69	2.81	2.73	2.64
Average Cu-Cu	2.94	3.13	2.93	2.65
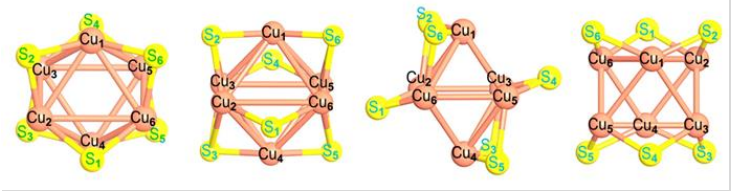				
S1-Cu2	2.27	2.29	2.26	2.36
S1-Cu6	2.27	2.25	2.27	2.36
S2-Cu1	2.22	2.22	2.23	2.36
S2-Cu2	2.22	2.21	2.23	2.36
S3-Cu3	2.22	2.24	2.23	2.36
S3-Cu4	2.24	2.29	2.23	2.36
S4-Cu3	2.27	2.25	2.27	2.36
S4-Cu5	2.27	2.29	2.26	2.36
S5-Cu4	2.22	2.22	2.23	2.36
S5-Cu5	2.22	2.21	2.23	2.36
S6-Cu1	2.24	2.29	2.23	2.36
S6-Cu6	2.22	2.24	2.23	2.36
Average S-Cu	**2.24**	**2.25**	**2.24**	**2.36**

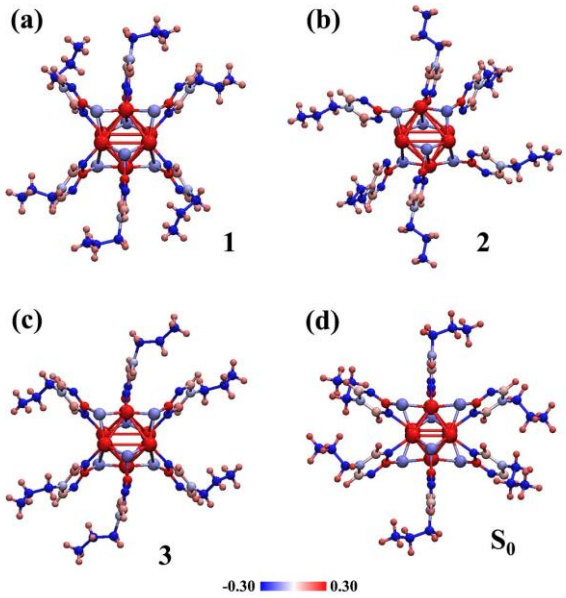

Fig. S5 The natural population analysis (NPA) charge distributions in single-crystals 1-3 (a-c) and DFT-optimized S_0 minima (d), respectively.

Table S3 DFT computed natural population analysis (NPA) charges distributions in single-crystals 1-3 and optimized at the S_0 minima, respectively.

Atoms	NPA			
	In **1**	In **2**	In **3**	DFT-optimized
Cu1	0.34	0.37	0.33	0.34
Cu2	0.33	0.38	0.33	0.34
Cu3	0.33	0.33	0.33	0.33
Cu4	0.34	0.37	0.33	0.34
Cu5	0.33	0.38	0.33	0.34
Cu6	0.33	0.33	0.33	0.33
Summary of Cu_6	**1.99**	**2.16**	**1.98**	**2.01**
S1	-0.17	-0.17	-0.17	-0.17
S2	-0.15	-0.16	-0.15	-0.17
S3	-0.15	-0.19	-0.16	-0.17
S4	-0.17	-0.17	-0.17	-0.17
S5	-0.15	-0.16	-0.15	-0.17
S6	-0.15	-0.19	-0.16	-0.17
Summary of 6S	-0.93	-1.04	-0.95	-1.01
Summary of 12N	-6.43	-6.45	-6.43	-6.50
Summary of 42C	-3.98	-3.98	-3.92	-6.25
Summary of 54H	9.36	9.32	9.33	11.75
Summary of $(SMPP)_6$	**-1.99**	**-2.16**	**-1.98**	**-2.01**

3.2 TD-DFT calculations

Table S4 TD-B3LYP computed wavelengths (nm, eV in brackets), oscillator strengths, and electronic configurations weights of strong electronic excitation transitions at the optimized $\mathbf{S_0}$ minimum.

Wavelength	Oscillator strength	Electronic configurations weights (in %)
289.20 (4.29)	0.1804	HOMO-2 → LUMO+12 (65.1)
288.97 (4.29)	0.1725	HOMO-3 → LUMO+12 (63.5)
251.55 (4.93)	0.0998	HOMO-6 → LUMO+12 (18.4) HOMO-10 → LUMO+10 (16.5) HOMO-10 → LUMO+9 (13.5) HOMO-9 → LUMO+10 (12.9) HOMO-7 → LUMO+12 (12.8)
251.51 (4.93)	0.1082	HOMO-10 → LUMO+10 (18.3) HOMO-7 → LUMO+12 (17.8) HOMO-6 → LUMO+12 (12.7) HOMO-10 → LUMO+9 (12.6) HOMO-9 → LUMO+9 (8.8)
244.70 (5.07)	0.0358	HOMO-9 → LUMO+11 (49.0) HOMO-16 → LUMO+1 (7.3)
244.63 (5.07)	0.0488	HOMO-10 → LUMO+11 (52.7)

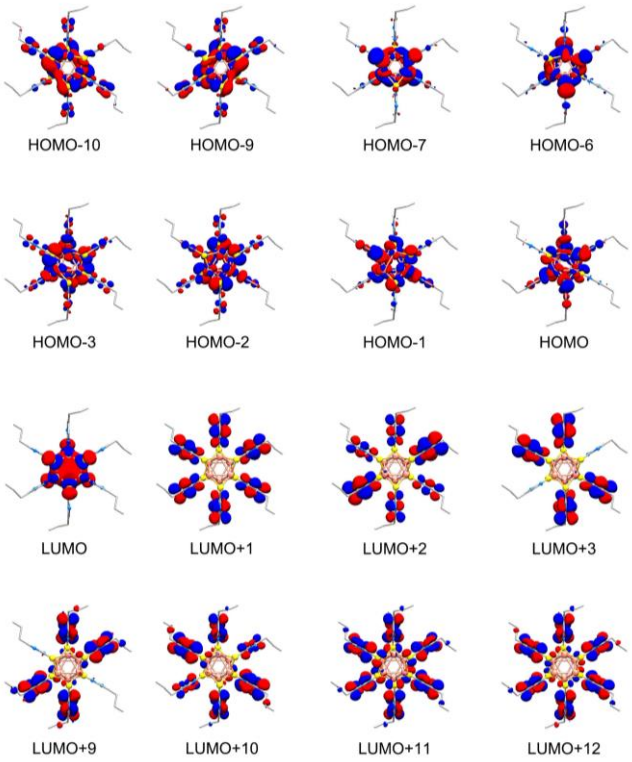

Fig. S6 TD-B3LYP calculated other canonical molecular orbitals (CMOs) at the $\mathbf{S_0}$ minimum of the $Cu_6(SMPP)_6$ cluster.

Table S5 TD-B3LYP computed wavelengths (nm, eV in brackets), oscillator strengths, and electronic configurations weights (in %) of strong electronic de-excitation transitions at the optimized $\mathbf{S_1}$ minimum of the $Cu_6(SMPP)_6$ cluster.

Wavelength	Oscillator strength	Electronic configurations weights (in %)
827 (1.47)	0.0245	LUMO → HOMO-1 (69.7)
396 (3.13)	0.0916	LUMO → HOMO-22 (56.2)
319 (3.89)	0.2000	LUMO → HOMO-29 (54.5)

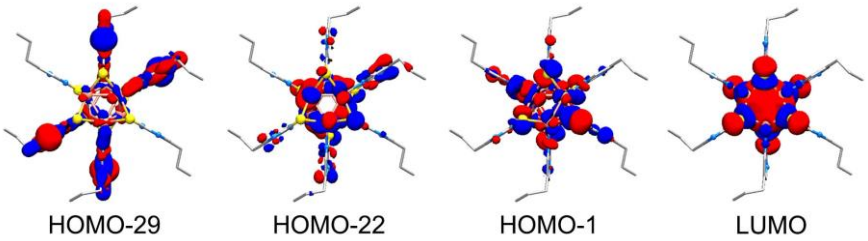

3.3 MO orbitals

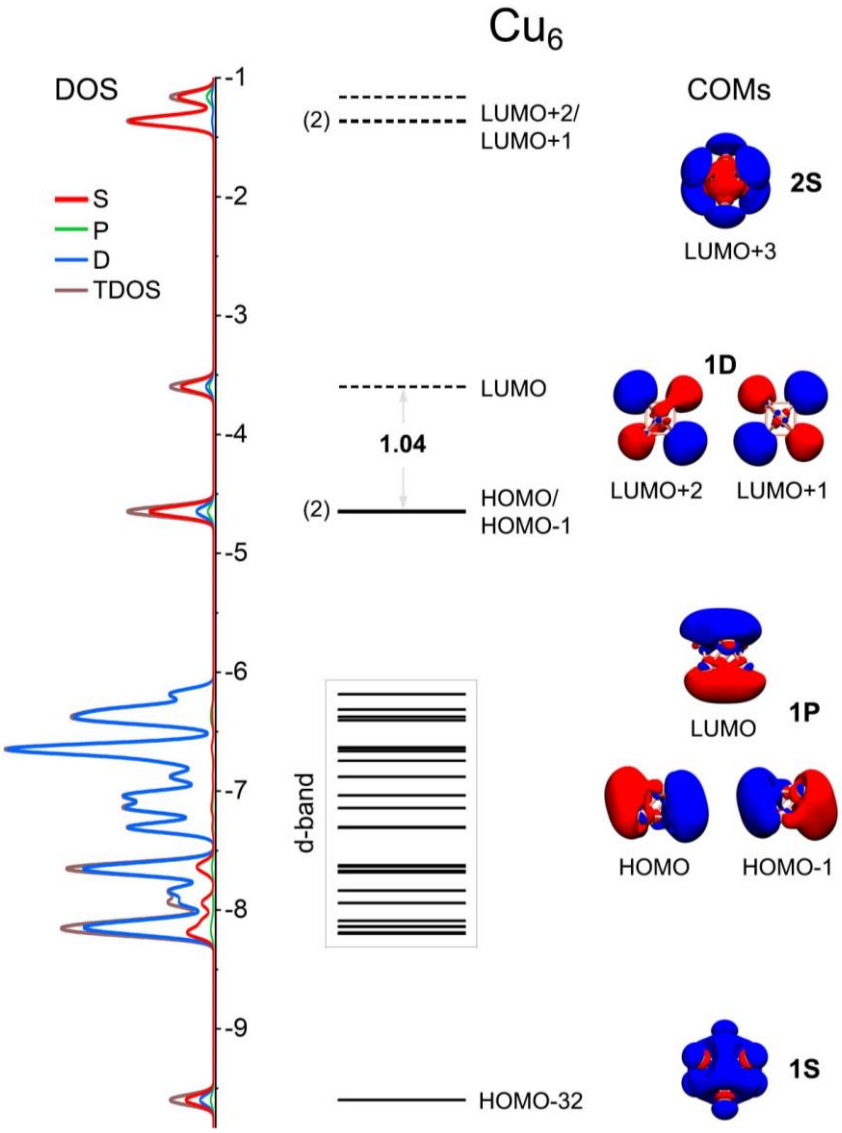

Fig. S7 Total and partial density of states (DOS), Kohn-Sham orbital energy levels and selected canonical molecular orbitals (COMs) of the optimized Cu_6 metallic core showing superatomic feature.

Table S6 Calculated molecular orbital energy and relevant weights with respect to Cu_6 and 6SMPP.

Orbitals	Energy (eV)	Weiths (%)	
		Cu_6	6SMPP
LUMO	-2.05	62.01	37.99
HOMO	-5.05	54.74	45.27
HOMO-1	-5.05	54.69	45.31
HOMO-2	-5.18	52.50	47.50
HOMO-3	-5.18	52.67	47.33
HOMO-4	-5.23	44.77	55.24
HOMO-5	-5.50	27.27	72.73
HOMO-6	-5.67	51.15	48.85
HOMO-7	-5.67	51.31	48.69
HOMO-8	-5.86	63.33	36.67
HOMO-9	-5.97	47.50	52.51
HOMO-10	-5.97	47.45	52.55
HOMO-11	-6.47	62.63	37.37
HOMO-12	-6.50	95.54	4.46
HOMO-13	-6.52	50.93	49.07
HOMO-14	-6.55	89.29	10.71
HOMO-15	-6.58	86.71	13.29
HOMO-16	-6.58	86.80	13.21
HOMO-17	-6.59	86.13	13.87
HOMO-18	-6.60	86.15	13.86
HOMO-19	-6.80	90.84	9.16
HOMO-20	-6.80	90.95	9.05
HOMO-21	-6.85	78.78	21.22
HOMO-22	-6.85	78.73	21.28
HOMO-23	-6.98	53.58	46.43
HOMO-24	-7.03	31.71	68.29
HOMO-25	-7.04	31.34	68.66
HOMO-26	-7.13	89.41	10.59
HOMO-27	-7.14	76.68	23.33
HOMO-28	-7.15	75.79	24.21
HOMO-29	-7.22	42.72	57.29
HOMO-30	-7.29	16.71	83.29
HOMO-31	-7.29	16.92	83.08
HOMO-32	-7.35	35.20	64.80
HOMO-33	-7.36	35.25	64.75
HOMO-34	-7.51	64.84	35.16
HOMO-35	-7.51	64.49	35.51
HOMO-36	-7.54	61.11	38.89
HOMO-37	-7.54	61.22	38.78
HOMO-38	-7.55	53.91	46.09
HOMO-39	-7.57	33.92	66.09
HOMO-40	-7.64	57.05	42.95
HOMO-41	-7.97	34.58	65.42
HOMO-42	-7.97	34.41	65.59
HOMO-43	-8.06	50.26	49.74
HOMO-44	-8.06	50.23	49.77
HOMO-45	-8.23	75.12	24.89
HOMO-46	-8.34	22.95	77.05
HOMO-47	-8.36	12.75	87.26
HOMO-48	-8.51	23.58	76.42
HOMO-49	-8.52	23.67	76.33
HOMO-50	-8.53	50.32	49.68
HOMO-51	-8.55	59.07	40.93
HOMO-52	-8.66	34.00	66.00
HOMO-53	-8.68	34.28	65.72

3.4 EDA-NOCV analysis

To unveil the bonding nature in $Cu_6(SMPP)_6$, we have conducted energy decomposition analysis (EDA),[7] which is known as a powerful tool to compare the nature of chemical bonds that are closely relevant. Based on the EDA, the total bonding energy can be divided into three parts:

$$\Delta E_{int} = \Delta E_{pauli} + \Delta E_{elstat} + \Delta E_{orb}$$

where ΔE_{pauli} is the repulsion energy caused by the Pauli exclusion principle, ΔE_{elstst} and ΔE_{orb} are the attraction energies due to electrostatic and orbital interactions, respectively. As presented by Table S7, the contribution of ΔE_{elstst} (-45.88 eV) to ΔE_{int} is slightly smaller than that of ΔE_{orb} (-50.83 eV). In other words, stabilization of $Cu_6(SMPP)_6$ mainly relies on the orbital hybridization bonding between metal core Cu_6 and six SMPP ligands. Further analysis based on natural orbitals for chemical valence (NOCV)[8] calculations suggests that the dominant pairwise orbital interaction to ΔE_{orb} (29.92 % contribution) comes from the hybridization of HOMO orbital (Cu_6) and LUMO+2 (six SMPP ligands), which yields HOMO-7 for the $Cu_6(SMPP)_6$ cluster.

Table S7 EDA-NOCV results for $Cu_6(SMPP)_6$ at the B3LYP/TZ2P level of theory using ADF, taking Cu_6 metal core and six SMPP ligands as interacting fragments. ‡The values in parentheses show the contribution to the total orital interaction ΔE_{orb}. Energy values are given in eV.

Energy term	Assignment	Interaction Fragments
		Cu_6 + 6SMPP
ΔE_{int}		-24.01
ΔE_{pauli}		72.70
ΔE_{elstst}		-45.88
ΔE_{orb}		-50.83
$\Delta E_{orb(1)}$‡	Cu_6 (HOMO-25/HOMO-32) → 6SMPP (LUMO+1) backdonation	-9.60 (18.89 %)
$\Delta E_{orb(2)}$‡	Cu_6 (HOMO) → 6SMPP (LUMO+2) backdonation	-15.21 (29.92 %)
$\Delta E_{orb(3)}$‡	Cu_6 (HOMO-1) → 6SMPP (LUMO) backdonation	-14.21 (27.96 %)
$\Delta E_{orb(4)}$‡	6SMPP (HOMO-7) → Cu_6 (LUMO) donation	-1.62 (3.19 %)
$\Delta E_{orb(5)}$‡	6SMPP (HOMO-6) → Cu_6 (LUMO+2) donation	-0.76 (1.50 %)
$\Delta E_{orb(6)}$‡	6SMPP (HOMO-1) → Cu_6 (LUMO+1) donation	-0.77 (1.51 %)
$\Delta E_{orb(rest)}$‡		-8.66 (17.03 %)

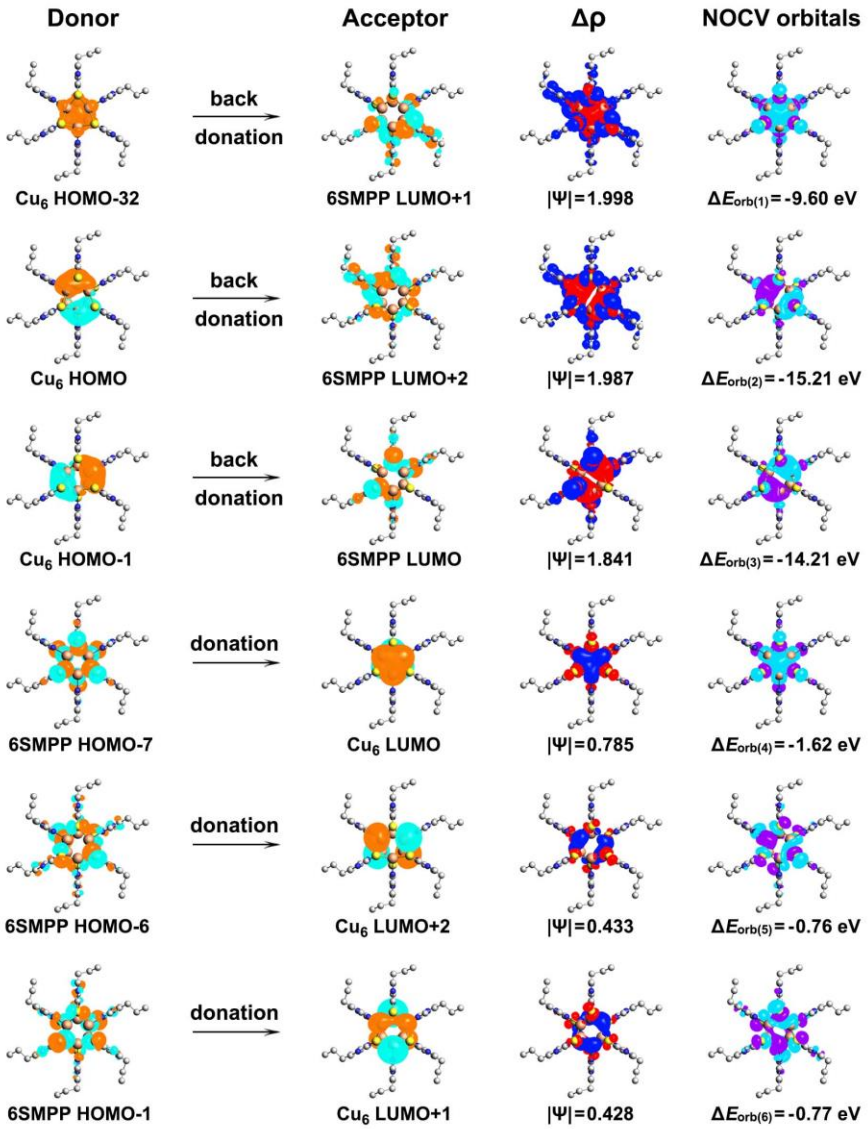

Fig. S8 The NOCV pairwise interactions, the corresponding deformation electron density plots Δρ and the corresponding NOCV pair of orbitals (ψ, eigenvalues given in parenthesis) between Cu_6 and 6SMPP fragments for $Cu_6(SMPP)_6$ at optimized S_0 minima using ADF. The Δρ is associated with the orbital interactions ΔE_{orb} of alpha electrons between two fragments in $Cu_6(SMPP)_6$. The colour code of the charge flow is from red to blue. The isosurface value is ±0.02 a.u. for orbitals and ψ, 0.0005 a.u. for Δρ, respectively.

References

1. S. Zhuang, L. Liao, J. Yuan, N. Xia, Y. Zhao, C. Wang, Z. Gan, N. Yan, L. He, J. Li, H. Deng, Z. Guan, J. Yang and Z. Wu, *Angew. Chem. Int. Ed.*, 2019, **58**, 4510-4514.
2. M. J. Frisch, G. W. Trucks, H. B. Schlegel, G. E. Scuseria, M. A. Robb, J. R. Cheeseman, G. Scalmani, V. Barone, B. Mennucci, G. A. Petersson, H. Nakatsuji, M. Caricato, X. Li, H. P. Hratchian, A. F. Izmaylov, J. Bloino, G. Zheng, J. L. Sonnenberg, M. Hada, M. Ehara, K. Toyota, R. Fukuda, J. Hasegawa, M. Ishida, T. Nakajima, Y. Honda, O. Kitao, H. Nakai, T. Vreven, J. A. Montgomery, Jr., J. E. Peralta, F. Ogliaro, M. Bearpark, J. J. Heyd, E. Brothers, K. N. Kudin, V. N. Staroverov, R. Kobayashi, J. Normand,

K. Raghavachari, A. Rendell, J. C. Burant, S. S. Iyengar, J. Tomasi, M. Cossi, N. Rega, J. M. Millam, M. Klene, J. E. Knox, J. B. Cross, V. Bakken, C. Adamo, J. Jaramillo, R. Gomperts, R. E. Stratmann, O. Yazyev, A. J. Austin, R. Cammi, C. Pomelli, J. W. Ochterski, R. L. Martin, K. Morokuma, V. G. Zakrzewski, G. A. Voth, P. Salvador, J. J. Dannenberg, S. Dapprich, A. D. Daniels, O. Farkas, J. B. Foresman, J. V. Ortiz, J. Cioslowski and D. J. Fox, 2009.

3. T. Lu and F.-W. Chen, *J. Comput. Chem.*, 2012, **33**, 580-592.
4. W Humphrey, A Dalke and K. Schulten, *J Mol Graph*, 1996, **14**, 33-38.
5. (a) E.J. Baerends, T. Ziegler, J. Autschbach, D. Bashford, A. Bérces, F.M. Bickelhaupt, C. Bo, P.M. Boerrigter, L. Cavallo, D.P. Chong, L. Deng, R.M. Dickson, D.E. Ellis, M. van Faassen, L. Fan, T.H. Fischer, C. Fonseca Guerra, M. Franchini, A. Ghysels, A. Giammona, S.J.A. van Gisbergen, A.W. Götz, J.A. Groeneveld, O.V. Gritsenko, M. Grüning, S. Gusarov, F.E. Harris, P. van den Hoek, C.R. Jacob, H. Jacobsen, L. Jensen, J.W. Kaminski, G. van Kessel, F. Kootstra, A. Kovalenko, M.V. Krykunov, E. van Lenthe, D.A. McCormack, A. Michalak, M. Mitoraj, S.M. Morton, J. Neugebauer, V.P. Nicu, L. Noodleman, V.P. Osinga, S. Patchkovskii, M. Pavanello, P.H.T. Philipsen, C. C. P. D. Post, W. Ravenek, J.I. Rodríguez, P. Ros, P.R.T. Schipper, H. van Schoot, G. Schreckenbach, J.S. Seldenthuis, M. Seth, J.G. Snijders, M. Solà, M. Swart, D. Swerhone, G. te Velde, P. Vernooijs, L. Versluis, L. Visscher, O. Visser, F. Wang, T.A. Wesolowski, E.M. van Wezenbeek, G. Wiesenekker, S.K. Wolff, T.K. Woo and A. L. Yakovlev, ADF2021, SCM, Theoretical Chemistry, http://www.scm.com/, 2021); (b) E. van Lenthe and E. J. Baerends, *J. Comput. Chem.*, 2003, **24**; (c) G. te Velde, F.M. Bickelhaupt, S.J.A. van Gisbergen, C. Fonseca Guerra, E.J. Baerends, J.G. Snijders and T. Ziegler, *J. Comput. Chem.*, 2001, **22**, 931-967; (d) C. Fonseca Guerra, J. G. Snijders, G. te Velde and E. J. Baerends, *Theor. Chem. Acc.*, 1998, **99**, 391-403.
6. T.-A. D. Nguyen, A. W. Cook, G. Wu and T. W. Hayton, *Inorg. Chem.*, 2017, **56**, 8390-8396.
7. (a) F. M. Bickelhaupt and E. J. Baerends, *Rev. Comput. Chem.*, 2000, **15**, 1-86; (b) M. V. Hopffgarten and G. Frenking, *Wiley Interdiscip. Rev.-Comput. Mol. Sci.*, 2012, **2**, 43-62; (c) T. Ziegler and A. Rauk, *Theor. Chim. Acta*, 1977, **46**, 1-40.
8. (a) M. Mitoraj and A. Michalak, *J. Mol. Model.*, 2007, **13**, 347-355; (b) A. Michalak, M. Mitoraj and T. Ziegler, *J. Phys. Chem. A*, 2008, **112**, 1933-1939; (c) M. P. Mitoraj, A. Michalak and T. Ziegler, *J. Chem. Theory Comput.*, 2009, **5**, 962-975.